Technology in Cancer Research & Treatment
2016, Vol. 15(6) NP47–NP60

DOI: 10.1177/1533034615615249
tct.sagepub.com

Emerging Role of MRI for Radiation Treatment Planning in Lung Cancer

David C. P. Cobben, MD, PhD[1], Hans C. J. de Boer, MSc, PhD[1], Rob H. Tijssen, MSc, DPhil[1], Emma G. G. M. Rutten, MSc, MD[1], Marco van Vulpen, MD, PhD[1], Jurgen Peerlings, MSc, PhD[2], Esther G. C. Troost, MD, PhD[2,3,4,5], Aswin L. Hoffmann, MSc, PhD[2,3,4,5], and Astrid L. H. M. W. van Lier, MSc, PhD[1]

Abstract

Magnetic resonance imaging (MRI) provides excellent soft-tissue contrast and allows for specific scanning sequences to optimize differentiation between various tissue types and properties. Moreover, it offers the potential for real-time motion imaging. This makes magnetic resonance imaging an ideal candidate imaging modality for radiation treatment planning in lung cancer. Although the number of clinical research protocols for the application of magnetic resonance imaging for lung cancer treatment is increasing (www.clinicaltrials.gov) and the magnetic resonance imaging sequences are becoming faster, there are still some technical challenges. This review describes the opportunities and challenges of magnetic resonance imaging for radiation treatment planning in lung cancer.

Keywords

MRI, lung cancer, radiation treatment planning

Abbreviations

ADC, apparent diffusion coefficient; bSSFP, balanced steady-state free precession; CT, computed tomography; DCE-MRI, dynamic contrast-enhanced MRI; 2D, 2-dimensional; 4D-CT, 4-dimensional computed tomography; DW-MRI, diffusion-weighted MRI; DWI, diffusion-weighted imaging; ECG, electrocardiogram; FLASH, fast low-angle shot; ^{18}FDG, ^{18}F-fluorodeoxyglucose; GTV, gross tumor volume; HP, hyperpolarized; IMRT, intensity-modulated radiation therapy; ITV, internal target volume; κ, inter-observer agreement; MRA, magnetic resonance angiography; MRI, magnetic resonance imaging; MR-linac, MRI linear accelerator; NSCLC, non–small-cell lung cancer; OARs, organs at risk; OS, overall survival; RD-MRI, respiratory dynamic MRI; PERCIST, PET response criteria; PET-CT, positron emission tomography–computed tomography; PFS, progression-free survival; PTV, planning target volume; rDOR, relative diagnostic odds ratio; RECIST, response evaluation criteria in solid tumors; RILT, radiation-induced lung toxicity; SBRT, stereotactic body radiotherapy; SNR, signal-to-noise ratio; SS-TSE-HF, thin-section single-shot turbo spin echo with half-Fourier acquisition; STIR-TSE, short tau inversion recovery turbo spin echo; SUV_{max}, maximum standardized uptake volume; TSE, turbo spin echo; T1w, T1-weighted; T2w, T2-weighted; USPIO, ultrasmall superparamagnetic iron oxide; UTE, ultrashort echo time; VMAT, volumetric-modulated arc therapy; ZTE, zero echo time

Submitted: July 10, 2015; Accepted: October 1, 2015.

[1] Department of Radiation Oncology, University Medical Center, Utrecht, the Netherlands
[2] Department of Radiation Oncology, MAASTRO Clinic, GROW—School for Oncology and Developmental Biology, Maastricht University Medical Centre, Maastricht, the Netherlands
[3] Helmholtz-Zentrum Dresden-Rossendorf, Dresden, Germany
[4] OncoRay, National Center for Radiation Research in Oncology, Dresden, Germany
[5] Department of Radiation Oncology, Medical Faculty and University Hospital Carl Gustav Carus, Technische Universität Dresden, Dresden, Germany

Corresponding Author:
David C. P. Cobben, MD, PhD, Department of Radiation Oncology, University Medical Center Utrecht, Heidelberglaan 100, 3584 CX Utrecht, the Netherlands.
Email: david.cobben@outlook.com

Introduction

The prognosis for patients with non-small cell lung cancer (NSCLC) remains poor.[1] Advances in imaging and radiation treatment delivery techniques are expected to improve disease-specific and overall survival (OS).[2] New imaging techniques focus on improving visualization of the primary tumor, affected regional lymph nodes, possible distant metastases, and organs at risk (OARs). The introduction of new radiation treatment strategies includes accelerated or dose-enhanced radiotherapy or particle beam therapy. The combination of these improved imaging and treatment techniques is aimed at increasing the dose to the treatment volume(s), while sparing the OAR, that is, increasing the therapeutic ratio.[3] Ultimately, this should lead to higher locoregional control with less toxicity and eventually to a better disease-specific and OS rate.

Several preliminary reports are available, which indicated that the above-mentioned efforts are worthwhile. It has been shown that patients with stage I to III NSCLC benefit from dose escalation through improved locoregional control and survival, with acceptable acute and late toxicity.[4-10] The hypothesis that dose escalation to the primary tumor in nonmetastatic NSCLC may lead to an increase in OS was confirmed in a meta-analysis.[11,12] Based on these initial results, the Radiation Therapy Oncology Group 0617 and several phase 1 and 2 studies were designed, which investigated dose escalation in stage II to III NSCLC (NCT01577212, 01629498, 01657617, 01024829, 01576796, and 01711697; ClinicalTrials.gov).[13,14] In the coming years, the final results of these studies should provide more insight into the clinical outcome of dose escalation in NSCLC.

Although dose escalation and stereotactic body radiotherapy (SBRT) for centrally located NSCLC have been applied, there are concerns about the acute and late pulmonary and cardiovascular toxicity, especially for patients with a medical history of cardiovascular and/or pulmonary disease.[15-19] From preclinical and clinical research, a complex interaction between the radiation dose to the lungs and the heart has been established, which can result in radiation-induced lung toxicity (RILT) and/or cardiac toxicity.[17,20,21] Next to the current dose constraints to the lung, the need for more stringent dose constraints to (specific parts of) the heart could play an important role in preventing cardiac toxicity and RILT.

To enable dose escalation with an acceptable toxicity profile, new imaging techniques were introduced for accurate definition and motion characterization of the primary tumor, of the involved regional lymph nodes, and of the OARs. Over the past years, positron emission tomography–computed tomography (PET-CT) and 4-dimensional computed tomography (4D-CT) were introduced for improved radiation target delineation and treatment planning.[22] For online position verification, in-room cone beam CT is rapidly becoming the new standard.[23]

In addition to new imaging techniques, new dose delivery strategies were introduced such as intensity-modulated radiation therapy (IMRT) and volumetric-modulated arc therapy (VMAT). The IMRT and VMAT increase the conformality of the dose distribution to the target volumes and hence enable decreasing the dose in the OARs.[3] In addition, intensity-modulated proton therapy is currently being investigated, although particular challenges due to range uncertainties can be expected for lung treatments.[24,25]

Despite the implementation of the aforementioned strategies, considerable uncertainties in tumor boundaries and motion remain, which require large planning margins and thus correspondingly large treatment volumes (planning target volume [PTV]).[26] These large treatment volumes, usually derived from population-based knowledge of required margins, lead to OAR doses that hamper more aggressive treatment strategies and induce considerable toxicity. An imaging modality providing excellent soft-tissue contrast and real-time continuous and detailed motion characterization may lead to a more accurate gross tumor volume (GTV) definition and individualized motion tracking for primary tumor, lymph nodes, and OARs. This allows for the reduction in both systematic and random errors and hence leads to significantly smaller, individualized margins and consequently individualized dose optimization.

Magnetic resonance imaging (MRI) seems to fulfill all these criteria: it provides excellent soft-tissue contrast and specific scanning sequences, which enable differentiation between different adjacent tissues. Furthermore, it allows for detailed motion characterization of all involved structures.[27-34] In this review, we will describe the current imaging techniques used for the radiation treatment planning in patients with lung cancer and discuss what role MRI might play in improving the definitions of GTV, clinical target volume, PTV, and OARs.

Detection of Primary Tumor

^{18}F-Fluorodeoxyglucose- (^{18}FDG)PET-CT is the imaging modality most widely used to distinguish a benign from a malignant solitary pulmonary nodule.[35] In addition, ^{18}FDG-PET-CT is often used to distinguish tumor from atelectasis.[36] In both cases, ^{18}FDG-PET-CT is used to define the GTV of the tumor as accurately as possible. However, ^{18}FDG-PET-CT also inherits significant limitations, being (1) limited spatial resolution hampering accurate target volume delineation, (2) window-width/window-level settings susceptible to interobserver variation, (3) blurring and misregistration of the PET images with the CT images due to organ motion (eg, heart and respiratory motion), and (4) false-positive findings caused by inflammatory processes.[3,35,37-39] Magnetic resonance imaging has the potential to overcome these limitations by supplying high-resolution high-contrast anatomical and (semi)-quantitative information on, for example, cell density or vascularization. In the next 2 paragraphs, the recent developments in MRI to distinguish malignant from benign tissue and to determine the extent of the tumor are described (Table 1).

Malignant Versus Benign

Magnetic resonance imaging is expected to play an increasingly important role in differentiating between malignant and

Table 1. Summary of MRI Sequences Per Indication.

Indication	Sequences	References
Tumor		
Malign versus benign	DCE, DWI, T2w	40-48
Invasion	RD, T2w, T1w + contrast, (ECG-triggered) MRA, SS-TSE-HF, UTE, 2D cine MRI	30,49-53
Lymph nodes		
Malign versus benign	DWI, STIR-TSE, USPIO	54-59
OARs		
Mediastinum, spinal cord, brachial plexus, (functional) lung tissue	T1w, T2w, bSSFP, HP-MRI	60-65
Motion (tumor, lymph nodes, and OARs)		
	bSSFP, FLASH, T2-TSE (2D cine MRI or 4D-MRI)	27-30,61,66-69

Abbreviations: bSSFP, balanced steady-state free precession; 2D, 2-dimensional; DCE, dynamic contrast enhanced; DWI, diffusion-weighted imaging; ECG, electrocardiogram; FLASH, fast low-angle shot; HP-MRI, hyperpolarized gas magnetic resonance imaging; MRA, magnetic resonance angiography; MRI, magnetic resonance imaging; RD, respiratory dynamic; SS-TSE-HF, thin-section single-shot turbo spin echo with half-Fourier acquisition; STIR-TSE, Short tau inversion recovery turbo spin echo; TSE, turbo spin echo; T1w, T1-weighted; T2w, T2-weighted; USPIO, ultrasmall superparamagnetic iron oxide; UTE, ultrashort echo time.

benign nodules. Zou *et al* showed that for dynamic contrast-enhanced MRI scans (DCE-MRI), the uptake pattern of contrast agents varied for the 3 pathologies.[40] Benign nodules showed a low overall uptake, whereas the uptake in both malignant and inflammatory nodules was initially high. However, 4 minutes after administration of the contrast bolus, the uptake in the inflammatory nodules was significantly higher than in the malignant nodules, possibly caused by differences in the vascular integrity. Besides DCE-MRI, diffusion-weighted imaging (DWI) may be used to differentiate malignant from benign nodules. This was confirmed in a meta-analysis, which also highlighted the need for standardization in future studies.[41] Furthermore, a study by Zhang *et al*[42] showed that the apparent diffusion coefficient (ADC) value, which can be derived from diffusion-weighted MRI (DW-MRI), is a significantly better discriminator of malignant and benign nodules than the maximum standardized uptake value in PET imaging (SUV_{max}). Similar results were found in other studies.[43-45] Due to the high DWI contrast between the malignant nodules and the other tissues, Chetley Ford *et al* claimed that DW-MRI may be a good tool for involved lymph node delineation[46] (Table 1).

Magnetic resonance imaging may also be used to discriminate atelectasis from the primary lung tumor. In T2-weighted (T2w) scans, a contrast difference can be observed between the tumor and the atelectasis.[47] This contrast difference is less well defined in T1-weighted (T1w) scans. Furthermore, atelectasis may be visualized with DWI. Yang *et al* performed DWI on patients with pathologically proven lung cancer and presence of atelectasis.[48] Region of interest analysis showed that the ADC of lung tumors was significantly lower than for atelectasis. An overview of T1w, T2w, DWI, and ADC images is shown in Figure 1. Unfortunately, neither ^{18}FDG-PET-CT nor MRI has been (prospectively) evaluated with histopathological conformation to distinctively discern between malignant tumor and atelectasis.

Tumor Extension

The extent of primary tumor invasion into mediastinal structures, the thoracic wall, or neurovascular structures is important for primary tumor staging and for the definition of the GTV in subsequent radiation treatment planning. The ''standard'' anatomical sequences used are T2w, T1w with contrast, and magnetic resonance angiography (MRA).[49,70] However, MRI can also be used to assess tumor invasion into mediastinal structures, either by enhancing existing sequences, such as MRA, or new sequences such as respiratory dynamic MRI (RD-MRI) and thin-section single-shot turbo spin echo with half-Fourier acquisition (SS-TSE-HF or HASTE) as demonstrated in 3 recently published articles.[50-52] More recently, imaging sequences with ultrashort echo time (UTE) are being explored to accurately discriminate between the tumor and the lung tissue[30] (Table 1).

Interpretation of thoracic MRA images is hampered by cardiac motion artefacts. Ohno *et al* enhanced the image quality of MRA using electrocardiogram (ECG) triggering.[33] In 20 of the 50 patients having NSCLC with tumor invasion into the mediastinum or hilum, image quality and diagnostic accuracy of the conventional MRA and ECG-triggered MRI were compared with contrast-enhanced CT and the surgical findings. The image quality of the ECG-triggered MRA images was significantly better than that of images acquired with conventional MRA or contrast-enhanced CT. In addition, ECG-triggered MRI showed a higher diagnostic accuracy for invasion of the pulmonary artery or vein of 86%, whereas contrast-enhanced CT, conventional MRI, and MRA demonstrated an accuracy of 68%, 73%, and 82%, respectively. In this study, however, a single-detector helical CT was used, which is not the current standard.

In 3 recently published articles, new MRI scan protocols were investigated.[51,52,71] Patients with resectable NSCLC underwent preoperative MRI and CT scans. The first 2 articles investigated RD-MRI, whereas the third article explored the use of SS-TSE-HF.[51,52,71] In each article, the new MRI technique was either added to conventional MRI sequences and compared with CT or directly compared with CT. Next, the radiological findings were then compared with the pathological findings of the surgical specimens.

The RD-MRI method visualizes the natural sliding motion of the lung tissue along the adjacent tissue. Patients breathed slowly during image acquisition. In patients with tumors showing no or restricted sliding motion, invasion of the tumor in the adjacent tissue was suspected.[50,52] Both CT and conventional MRI already showed sensitivity and negative predictive value of 100% for tumor invasion. However, the specificity of CT

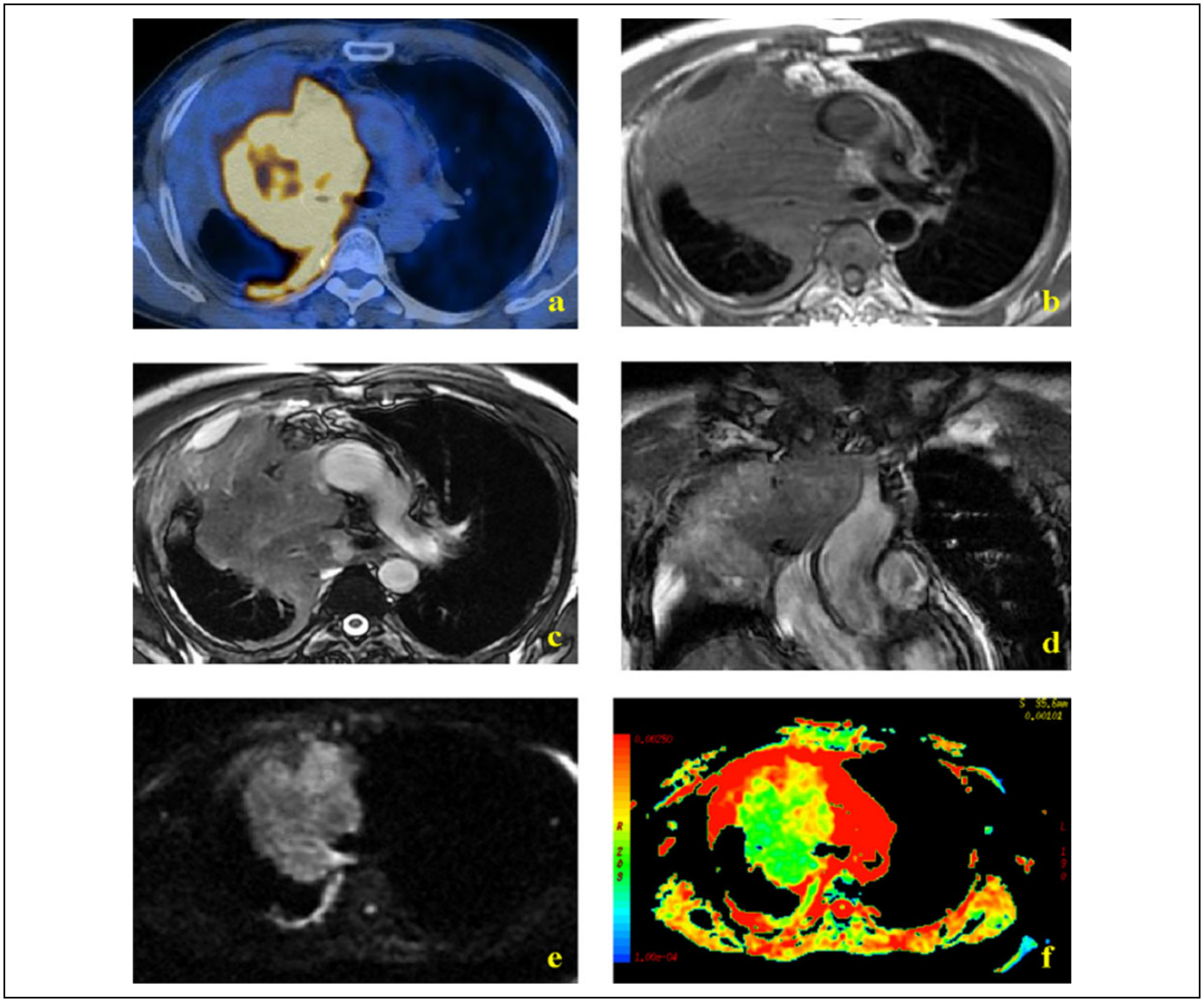

Figure 1. Overview of various MRI contrasts. A, PET/CT, (B) T1w MRI, (C and D) T2w MRI, (E) DWI (b = 500 s/mm^2), and (F) ADC map. Reprinted with permission from Yang *et al*.[48] ADC indicates apparent diffusion coefficient; DWI, diffusion-weighted imaging; MRI, magnetic resonance imaging; PET-CT, positron emission tomography–computed tomography; T1w, T1-weighted; T2w, T2-weighted.

was generally low. The advantage of RD-MRI is that it significantly lowers the number of false-positive findings and thereby increases the specificity as compared to CT and/or conventional MRI sequences. This led to an increase in specificity in both studies of 29% to 71% and 44% to 69%, respectively.[52,71]

The RD-MRI is particularly accurate for tumors that are less than 5 cm in diameter and tumors close to the mediastinum. There are 3 possible explanations.[50] First, the lower lobes show more respiratory movement than the upper lobes and therefore possess more "sliding" motion potential with the tumor. Second, a tumor larger than 10 cm and close to the chest wall exhibits little motion, for the weight of the tumor hinders motions between the tumor and the adjacent tissue. Third, in the upper lobes, especially the left upper lobe, there is little room for movement because of the tight anatomical configuration.

The SS-TSE-HF MRI has a tissue contrast comparable with turbo spin echo. However, by obtaining 3-mm slices with parallel imaging perpendicular to the tumor, the spatial resolution can be increased, a technique also known as SS-TSE-HF MRI (Figure 2).[51] A breath hold of 12 seconds is needed to acquire a full data set. With this technique, the sensitivity for local invasion was 85%, which was comparable with CT and "conventional" MRI (RD-MRI, conventional axial SS-TSE-HF MRI, and T1w high-resolution isotropic volume excitation). Remarkably, the specificity was 89% and thus superior to the rates of 26% and 61% for CT and conventional MRI sequences, respectively. Furthermore, the 2 reviewers who independently reviewed the imaging modalities, both blinded for clinical

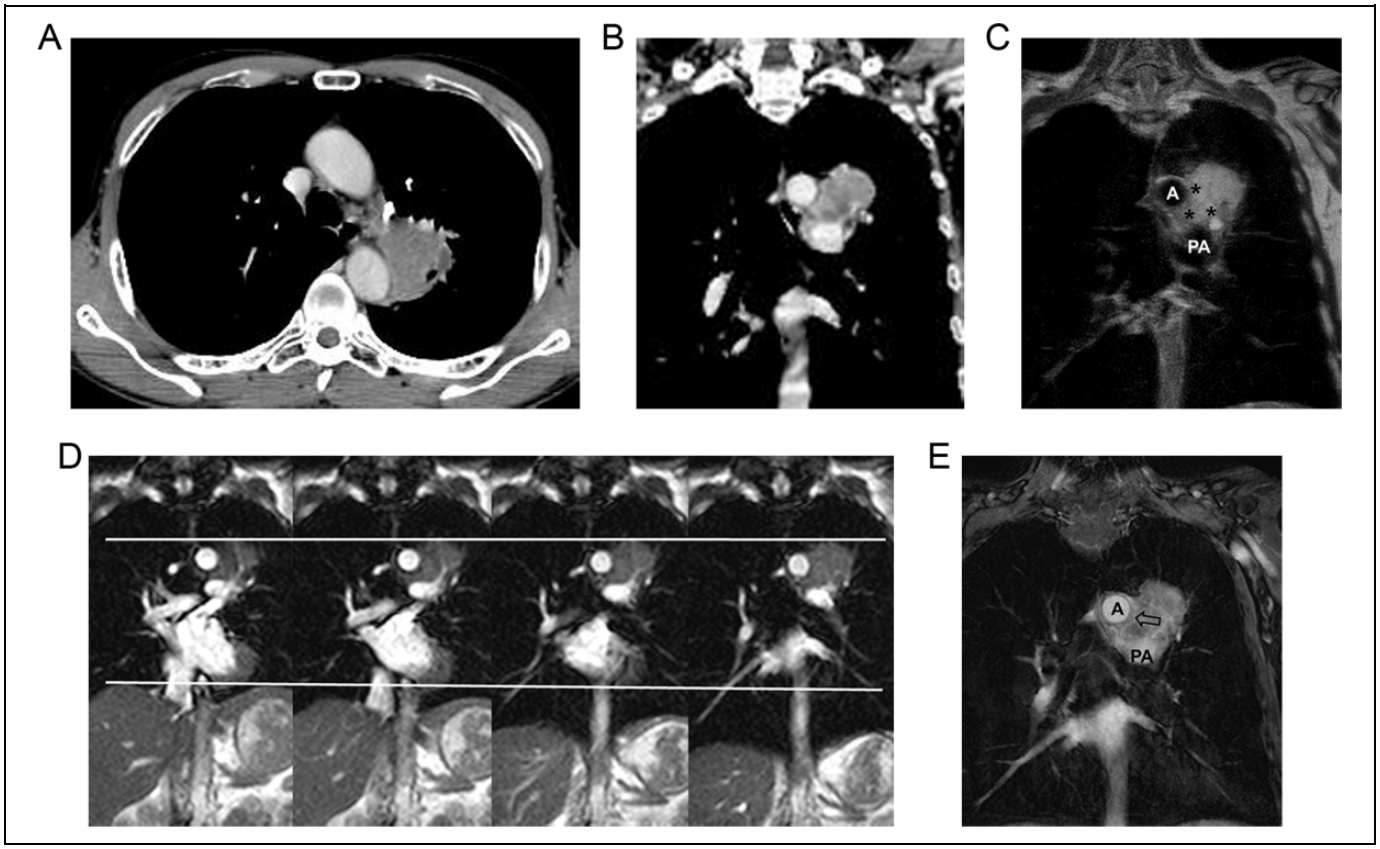

Figure 2. A 57-year-old male with adenocarcinoma abutting the aorta and pulmonary artery. A, An axial CT image shows a 170° contact angle between the mass and the aorta with 4 cm in extent of contact area. B, A coronal reformatted CT image shows the mass also abuts the pulmonary artery with a 110° contact angle with 3.5 cm in extent. C. An SS-TSE-HF image shows protrusion of the mass into the mediastinal fat suggesting invasion. However, the low-signal line around the tumor (asterisks) and the margins of the aorta and pulmonary artery are intact. D, On dynamic MRI, there is no sliding motion of the tumor (superior white line) at the mediastinum, aorta, or pulmonary artery during respiration (inferior white line, diaphragm motion). E, A THRIVE image shows a clear margin of the pulmonary artery, suggesting no invasion, but asymmetric thickening of aortic margin, which indicates invasion. Therefore, tumor invasion was suspected at the mediastinal fat and aorta, without invasion of the pulmonary artery on conventional MRI. During surgery, it was found that the tumor had invaded only into the mediastinal fat, with negative surgical margin on pathologic findings. Reprinted with permission from Chang *et al*.[51] A indicates aorta; CT, computed tomography; MRI; magnetic resonance imaging; PA, pulmonary artery; SS-TSE-HF, thin-section single-shot turbo spin echo with half-Fourier acquisition; THRIVE, T1 high-resolution isotropic volume excitation.

information and the findings of the other imaging modalities, had an excellent interobserver agreement ($\kappa = 0.81$) when using thin-section SS-TSE-HF MRI as compared to conventional MRI ($\kappa = 0.68$) and CT ($\kappa = 0.54$).

Noteworthy, most patients in the 3 aforementioned studies had a tumor either with chest wall invasion or with invasion of the aorta. To our knowledge, little is known about sensitivity and specificity of (those) MRI sequences with regard to invasion of the other mediastinal structures or the invasion in bony anatomy.

The last sequence, UTE, enables signal retrieval close to air–tissue transitions, which is problematic using other sequences.[30] With the UTE technique, the time between MRI signal generation and acquisition is extremely shortened in order to capture as much signal as possible. In one study, the UTE technique was optimized in healthy volunteers showing improved visualization of the lung tissue and airways.[30] Unfortunately, validation of UTE imaging against pathological specimens is still lacking. We anticipate that UTE imaging may be of special interest for radiation treatment planning as it can potentially lead to a more accurate depiction of the tumor borders.

Tumor Motion

Four-dimensional CT is the standard imaging modality for motion detection of primary lung tumors. A disadvantage is that it reconstructs motion as a function of the respiratory phase instead of time. Therefore, it does not reflect tumor motion accurately in real time.[26] Since tumor motion can differ significantly depending on the tumor location, it is important to have accurate motion characterization for accurate definition of the GTV and subsequent PTV margins.[26]

Motion characterization with MRI can be performed with cine MRI. With this technique, multiple 2-dimensional (2D) volumes per second can be acquired along any slice orientation,

and image data are very rapidly processed. Cine MRI can be complementary to 4D-CT. Cine MRI sequences show the motion pattern per respiratory cycle, whereas CT shows the average motion pattern over a number of respirations.[72] Therefore, cine MRI is a more direct measure of respiratory motion and can also be used to gain insight into the variation in the respiratory pattern. This technique has already shown to accurately depict impaired respiratory mechanics associated with pulmonary emphysema.[27] Important to remember is that dynamic sequences always have a tradeoff between temporal and spatial resolution. The search for new dynamic sequences is to find an ideal balance between temporal and spatial resolution, which enables the radiation oncologist to accurately define the tumor as well as to determine the individual movement pattern of the tumor with respiration and possibly with cardiac motion (Table 1).

Two sequences for fast cine MRI have been investigated frequently: balanced steady-state free precession (bSSFP) and fast low-angle shot (FLASH) imaging.[28] In patients with stage I NSCLC, 2 dynamic MRI techniques were compared: 1 sequence with a high-spatial resolution (bSSFP, 3 images/s) and 1 with a high-temporal resolution (FLASH, 10 images/s).[28] The data acquisition rate was increased by parallel acquisition techniques. The bSSFP showed the best signal-to-noise ratio (SNR), with still an acceptable good temporal resolution. However, in this study, only the movement in the craniocaudal direction was investigated in the coronal plane, and a slice thickness of 10 mm was applied.

The use of 2D and 3-dimensional cine MRI for offline and online soft-tissue–based image guidance in patients with stage I to IV NSCLC is currently under investigation at the University of Texas Southwestern Medical Center (NCT01421784, ClinicalTrials.gov). This investigation focuses on monitoring moving and deforming tumors.

Lymph Nodes

^{18}F-fluorodeoxyglucose–PET-CT has a high negative predictive value for the detection of metastatic mediastinal lymph node in lung cancer, and is therefore the imaging modality of choice for hilar/mediastinal staging, in combination with histological or cytological confirmation.[35,38] However, inflammation and granulomatous reactions may lead to false-positive PET readings in regional lymph nodes, and (small) lymph nodes may be missed due to the low resolution and motion blurring.[38]

Various MRI techniques are available to visualize hilar/mediastinal lymph nodes in NSCLC. Good visualization of lymph nodes has been reported for fat-suppressed imaging with short tau inversion recovery turbo spin echo (STIR-TSE; Figure 3).[54] The signal intensity of the lymph nodes was found to be a good predictor of malignancy with a sensitivity of 90.1% and an accuracy of 92.2%.[54] Diffusion-weighted MRI has the potential to discriminate malignant from benign lymph nodes, although first results were contradictory.[55] In one study, the sensitivity and specificity for differentiation between malignant and benign lymph nodes of ^{18}FDG-PET-CT, STIR-TSE, and DW-MRI were found to be comparable.[55] Conversely, another study reported the detection and ADC analysis of small malignant lymph nodes originating from NSCLC to be impossible[56] (Table 1).

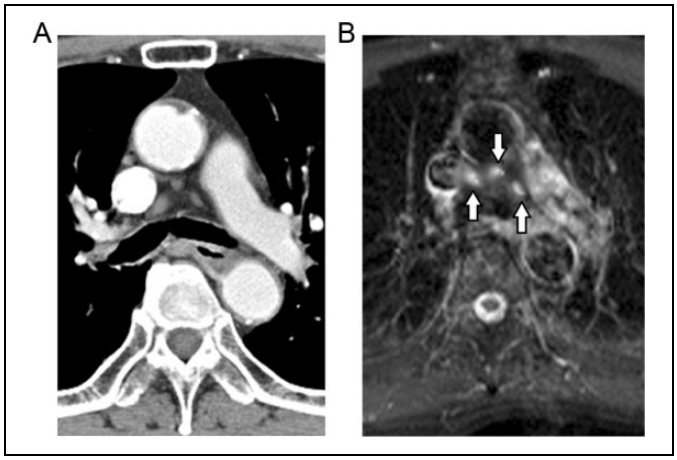

Figure 3. Three regional metastases in the lower paratracheal lymph nodes originating from an adenocarcinoma (indicated by 3 arrows). A, Contrast-enhanced CT scan. B, Transverse STIR-TSE. In the TSE sequence, a clearer contrast between mediastinal fat and surrounding tissue is generated. Reprinted with permission from Ohno *et al*.[54] CT indicates computed tomography; STIR-TSE, short tau inversion recovery turbo spin echo.

Peerlings *et al*[57] recently conducted a systematic meta-analysis on the diagnostic performance of MRI, validated against histology and/or cytology, for the detection of hilar/mediastinal lymphadenopathy in patients with NSCLC. Twelve studies fulfilled the eligibility criteria. On per-patient basis, sensitivity and specificity were 87% and 88%, respectively. On per-nodal basis, the measures were 88% and 95%, respectively. Subgroup analyses suggest greater diagnostic performance of quantitative evaluation over qualitative evaluation on both per-patient and per-nodal basis (relative diagnostic odds ratio [rDOR] = 2.76 and rDOR = 7.25; $P = .01$). These results were favorable when compared to 4 recent meta-analyses on ^{18}FDG-PET-CT reporting average sensitivity and specificity of 74% and 89% on per-patient basis and of 68% and 93% on per-nodal basis, respectively.[73-76]

Lymph Node Motion

Contrast-enhanced CT, registered to the ^{18}FDG-PET-CT, is the imaging standard for the delineation of the lymph nodes. However, accurate delineation of metastatic lymph nodes is hampered by 2 limitations. First, the movement of the lymph nodes, and second, the technical limitations of these imaging modalities (Table 1).

Several processes influence the movement of the lymph nodes. The respiratory pattern, cardiac motion, location of lymph nodes (eg, mediastinal vs hilar region), and changes in the lymph node volume during treatment influence the mobility

of the lymph nodes. Furthermore, movement of the metastatic lymph nodes hardly correlates with the movement of the tumor.[77,78] The movement of the lymph nodes aggravates the limitations of ^{18}FDG-PET-CT and contrast-enhanced CT: (small) nodes may be missed due to the low resolution and motion blurring.[38]

Cine MRI has the potential to characterize the motion of the lymph nodes. However, to our knowledge, no research on this subject has been published yet. We believe that the motion characterization of the tumor and lymph nodes will be essential in creating individualized PTV margins, enabling enhanced sparing of the OARs, and safer dose-escalation studies and stereotactic radiotherapy of centrally located tumors.

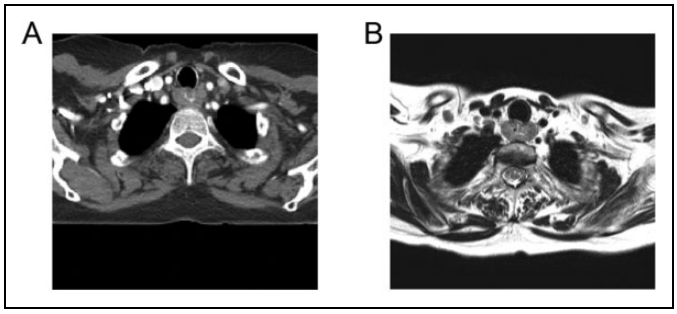

Figure 4. Computed tomography and MRI image of a 59-year-old female with a T3N1M0 squamous cell carcinoma of the proximal esophagus with a subcarinal metastatic lymph node. A, Contrast-enhanced CT scan. B, T2-weighted MRI scan. T2-weighted MRI shows the contour of the tumor more clearly than contrast-enhanced CT. Moreover, on T2w MRI, it is easier to distinguish between the different structures surrounding the tumor. For imaging parameters see Van Rossum *et al*.[79] CT indicates computed tomography; T2w, T2-weighted; MRI, magnetic resonance imaging.

Organs at Risk

The (contrast-enhanced) CT is the standard imaging modality for the delineation of the OARs, such as the lungs, spinal cord, esophagus, heart, large thoracic vessels (eg, aorta), trachea, bronchial tree, brachial plexus, spinal cord, and ribs.[60]

Several limitations hinder adequate delineation of some of these OARs. First, the current soft-tissue contrast provided by the contrast-enhanced CT makes it difficult to accurately delineate the esophagus, the outer wall of the vessels, and the contours of the heart. Second, as described earlier, the 4D-CT does not give an accurate reflection of the real-time motion of the OARs.

Although the MRI has better soft-tissue contrast than the contrast-enhanced CT, no publications are available on mediastinal MRI imaging. The University Medical Center Utrecht is currently investigating MRI sequences for esophageal cancer. T2-weighted images enabled a good contrast of the esophagus and aortic wall with the mediastinal fat and between the mediastinum and the lung tissue (see Figure 4). This contrast was improved when data acquisition was triggered on the respiratory phase. The imaging protocols for visualization of esophageal cancer are likely to be useful for anatomical imaging of the OARs in the mediastinum (Table 1).

Magnetic resonance imaging is already being used to depict the brachial plexus and spinal cord. It is advised to fuse the MRI with the CT for contouring of the brachial plexus and to use the spinal canal on CT for delineating the spinal cord.[60] Although the position of the thoracic spinal cord is relatively stable, accuracy within 0.5 mm, it is possible that tumors, approximating or extending into the vertebra, could have a benefit from (repeated or online) MRI.[61]

Organs at Risk Motion

The mobility of several OARs has been investigated with 4D-CT. An early study by Giraud *et al* showed that thoracic organs move considerably due to respiratory motion, especially at the diaphragm (up to 35 mm), whereas the smallest motion was recorded at the lung apices (5 mm).[80] The mobility of the esophagus, especially of the distal esophagus, can be as large as 9 mm in the dorsoventral or the lateral direction.[81] The motion of the heart has been investigated recently and can be as large as 13 mm in the lateral direction.[21]

No specific MRI sequences have been investigated to characterize the motion of the OARs for radiation treatment planning. This is unfortunate since acute and late cardiac and lung toxicity in thoracic radiotherapy is substantial, especially in patients with cardiac and pulmonary toxicity. Furthermore, SBRT of (central) lung tumors, dose-escalation studies, and new systemic therapies will probably lead to a longer survival and therefore also to an increase in observable late toxicity. Cine MRI will have an important role to characterize the real-time motion of the OARs, which may lower the dose in OARs when taken into account properly in treatment planning (Table 1). In addition, knowledge of the motion patterns will enable more realistic registration of the dose delivered to the OARs.

Technical Challenges

Although MRI is increasingly used to complement the image-guided radiation treatment planning process, there are still major challenges to overcome. Compared to other thoracic and abdominal imaging, lung imaging is the most challenging, mainly due to the presence of air in combination with respiratory and cardiac-induced motion (Table 1).

First of all, since the majority of the lung volume is air, the proton density in lung parenchyma is very low, and thus, very little signal is available for the MRI scanner to pick up.

Second, since air and tissue have varying magnetic susceptibility, the T2* of lung parenchyma is very short (1.0-2.5 ms).[82] The short T2* in combination with the low proton density makes the SNR in lungs typically very low compared to the SNR in other tissue types. For this reason, lung MRI sequences often require a few signal averages to produce images with sufficient image quality. On top of that, the magnetic susceptibility differences in air and tissue create local field

inhomogeneities around air–tissue interfaces. Functional imaging sequences such as DW-MRI are extremely sensitive to these magnetic field offsets and display large image distortions if not accounted for.

Respiratory and cardiac motion further complicates imaging of the lungs and mediastinal lymph nodes.[83] To prevent motion-induced image artifacts, for example, image blur or ghosting, lung MRI scans are often obtained with a breath hold protocol or performed in a gated (or triggered) fashion, such that data are only acquired during a quiescent portion of the respiratory or cardiac cycle. This, however, reduces the efficiency of data collection (the sequence is stopped for periods of time), resulting in rather lengthy examinations. This may pose problems for patients who are too frail to be in the scanner for a long time or unable to perform breath holds.

Finally, in the context of MRI-guided radiotherapy (ie, MR-linac–[MRI linear accelerator] based treatments), one will have to take into account the effect of the magnetic field on the dose delivery. The so-called electron return effect refers to the increased dose at tissue-to-air boundaries caused by returning secondary electrons that experience a torque (ie, Lorentz force) by the magnetic field.[84-87] Although this can be accounted for in treatment planning, one needs to assure that all air-to-tissue boundaries are visualized with great geometrical accuracy. To accomplish this, special sequences with ultrashort or even zero echo time (UTE and ZTE sequences, respectively) are needed that are fast enough to image the entire lungs in a feasible scan time.

Future Perspectives

Although the lung is one of the most challenging organs to image using MRI, the pace at which new techniques are being developed is high. In the next few paragraphs, we will discuss a few novel techniques that are likely going to have a significant impact on future radiotherapy imaging protocols. These techniques include custom sequences for motion management, improved use of functional imaging information, novel contrast agents in the form of hyperpolarized (HP) gas, ultrasmall superparamagnetic iron oxide (USPIO), and treatment response evaluation and prediction (Table 1).

Motion Management

The current standard of dealing with thoracic motion in (stereotactic) radiotherapy of lung tumors is an internal target volume (ITV)-based approach. The ITV is typically generated from the thoracic motion information obtained by 4D-CT. Although no vendor solution exists as of yet, several 4D methods for MRI have been developed in a research setting.[66,67,88] Apart from a few adaptations to cope with the technical differences between CT and MRI, these methods are comparable to the 4D-CT methods by the fact that they all sort the data based on the respiratory trace retrospectively. The advantage of 4D-MRI over 4D-CT is its flexibility in acquisition strategy, which can avoid some of the artifacts typically seen in 4D-CT such as motion-induced blurring and incomplete structure artifacts.[89] In addition to this, MRI has improved soft-tissue contrast, which can be tuned to either the tumor or the surrounding OARs. Because of these advantages, we foresee that vendors will also turn 4D-MRI into product within a few years' time.

Unfortunately, retrospective 4D methods hold 2 clear disadvantages: (1) they only provide a representation of the ''average'' tumor motion (ie, they do not provide information on the intercycle variability) and (2) the motion during simulation may be different from motion during the treatment fractions.[90] To mitigate these disadvantages, a few research groups have endeavored to develop techniques that link the simulation scans with the real-time imaging available during treatment.[88,91] The goal is to combine the high-resolution 4D information obtained during simulation with the fast, but often 2D, imaging during radiation in through physiological or mathematical motion models. In the future, this will lead to accurate dose optimization, taking 4D information into account.

Approaches have been explored in a conventional setting by linking 4D-CT to 2D electronic portal imaging device imaging or for future MRI-linac–based treatments linking 4D-MRI to real-time 2D cine MRI. All these methods aim to solve the fact that MRI is not fast enough to provide true 4D real-time imaging. However, over the last few years, tremendous advances have been made in imaging speed. These developments are likely to continue and promise even greater imaging speeds in the future and will hopefully bring true 4D real-time MRI within reach of clinical use.

Another interesting application of the recently developed motion models is the reconstruction of PET images in hybrid PET-MRI scanners. Using the simultaneously acquired MR images, it is possible to correct for motion blur of the PET acquisition, thereby increasing the PET resolution, as shown by several groups.[92,93] In the future, this could have a significant impact on the detection of small mediastinal lymph nodes.

New Developments in Functional Imaging

Apart from combined PET-MRI imaging, we anticipate further advances in multiparametric MRI. In other areas, such as prostate and brain imaging, it is common to acquire multiple quantitative MRI scans, such as DWI-MRI and DCE-MRI. Instead of utilizing each imaging sequence for individual purposes, the current efforts focus on advanced modeling techniques on multiparametric imaging, where the combined information from multiple contrasts is used for diagnosis, staging, and radiation treatment planning.[94-96] The complimentary information obtained by conventional T2w imaging (morphological information), combined with functional techniques such as DWI-MRI, and DCE-MRI has been very successful in imaging of the prostate. We anticipate that these sequences, in combination with RD-MRI, will be prime candidates for multiparametric MRI of the lung. However, a prerequisite for multiparametric MRI is accurate image registration between the different scans.

When imaging the lung, conventional DW-MRI and other functional sequences have large geometric distortions, making accurate registrations difficult. This is one of the technical challenges that have to be addressed before the added value of multiparametric MRI can be assessed in the context of lung imaging.

Hyperpolarized MRI

In order to overcome the low proton density in the lungs, HP gas MRI can be used. In HP-MRI, MRI-sensitive nuclei (eg, 3He or ^{129}Xe) are being polarized and administered to the patient during the scan. The hyperpolarization enables direct detection of the gas on MRI, which dramatically improves the SNR in the lung parenchyma and allows function assessment of the lungs. Several studies have already reported that HP-MRI provides additional information on healthy lung tissue in patients with NSCLC, and studies are being designed to investigate functional lung avoidance treatment planning based on HP-MRI.[62-64] If these trials are successful, this will eventually translate into the clinic.

Ultrasmall Superparamagnetic Iron Oxide

In the past decades, USPIO particles have been developed for diagnostic imaging, especially nodal staging.[58] One such particle is ferumoxytol. Under normal circumstances, ferumoxytol is taken up by macrophages in nonmalignant lymph nodes, which results in a change from hyperintense (white) into a hypointense (dark) lymph node on T2w (contrast-enhanced) images. If the lymph node contains metastatic cells, little or no ferumoxytol will be taken up and the (metastatic part of the) metastatic lymph node will remain hyperintense (white; Figure 5).[58,59]

Most research has been performed for the nodal staging in prostate cancer and shows a sensitivity between 65% and 92% and specificity between 93% and 99%.[98,99] To our knowledge, only one publication exists, in which MRI and ferumoxtran-10 were used for mediastinal staging in 18 patients with NSCLC.[100] The MRI findings were correlated with histological or cytological findings, and the authors reported an overall sensitivity of 92% and specificity of 80%. The sensitivity and specificity were dependent on the size of the lymph nodes, with a sensitivity and specificity of 67% and 88% in nodes <15 mm and 100% and 71% in nodes >15 mm, respectively. This may be explained by the limited resolution and other technical limitations of the MR scanners of that time period. Future research should focus on the comparison of ferumoxytol-enhanced MRI sequences with PET-CT and histological findings.

Treatment Evaluation and Prediction

Currently, the treatment response is assessed with the response evaluation criteria in solid tumors (RECIST version 1.1), which were last revised in 2009.[101] These criteria determine treatment response by changes in tumor size on CT in 2 dimensions. Three-dimensional or functional changes in the tumor (eg, measured with DWI-MRI, DCE-MRI, or PET-CT) were not incorporated in the revised RECIST criteria. This is a missed opportunity for 2 reasons. First, future evaluation tools should be aimed at detecting other signs of treatment response, such as functional imaging, since the use of targeted agents may not lead to significant reduction in tumor size and volumetric responses to chemoradiation do not correlate with pathological complete response.[102-104] Second, recent publications in patients with NSCLC indicate that metabolic volumetric information of the tumor (and metastatic lymph nodes and distant metastases), derived from either repeated ^{18}FDG-PET-CT for therapy evaluation or solely from diagnostic ^{18}FDG-PET-CT, can be highly predictive of survival even in patients with the same tumor, node, and metastasis stage.[105-108]

Although functional changes in tumor metabolism during treatment have been incorporated in the PET response criteria (PERCIST), PERCIST has only been validated for the treatment evaluation in lymphoma.[103,109] The main reasons for not using ^{18}FDG-PET-CT for treatment evaluation more widely are the limited availability of PET-CT and the lack of sufficient standardization.[109] International multicenter studies will probably accelerate the process of standardization.

Magnetic resonance imaging is increasingly investigated for therapy evaluation of neoadjuvant therapies to guide organ-preserving surgery in breast, rectal, and esophageal cancers.[79,110-113] Most clinical MRI studies concerning therapy evaluation for lung cancer used DW-MRI and demonstrated the potential of (early) therapy response evaluation and prediction.[114,115] Two studies used DW-MRI to assess the early treatment response and predict prognosis early during the treatment.[114,115] Yabuuchi *et al* analyzed 28 patients with stage IIIB and IV NSCLC who received platinum-based chemotherapy, performing a DW-MRI at baseline and after 1 course of chemotherapy. The ADC value increased during treatment and correlated significantly, with a decrease in tumor size on CT ($r2 = .41$). More importantly, the increase in ADC identified a good and poor prognostic group, which significantly correlated with the OS and progression-free survival (PFS).[115] Tsuchida *et al*[114] showed similar results in 28 patients with stage IIIB and IV NSCLC (n = 17) and small-cell lung cancer (n = 11) who received platinum-based chemotherapy and underwent DW-MRI and 18FDG-PET before and after 1 course of chemotherapy. The increase in ADC and SUV_{mean} was significantly correlated with responders and nonresponders (based on PFS and OS), as opposed to no significant correlation to the change in tumor diameter on CT. The results of these studies suggest that the ADC change precedes morphological changes (eg, "tumor shrinkage").

The first steps for the implementation of MRI for radiation treatment planning in lung cancer have been taken with the current MRI techniques. However, the focus of future research should be on image registration, image guidance, and treatment adaptation.

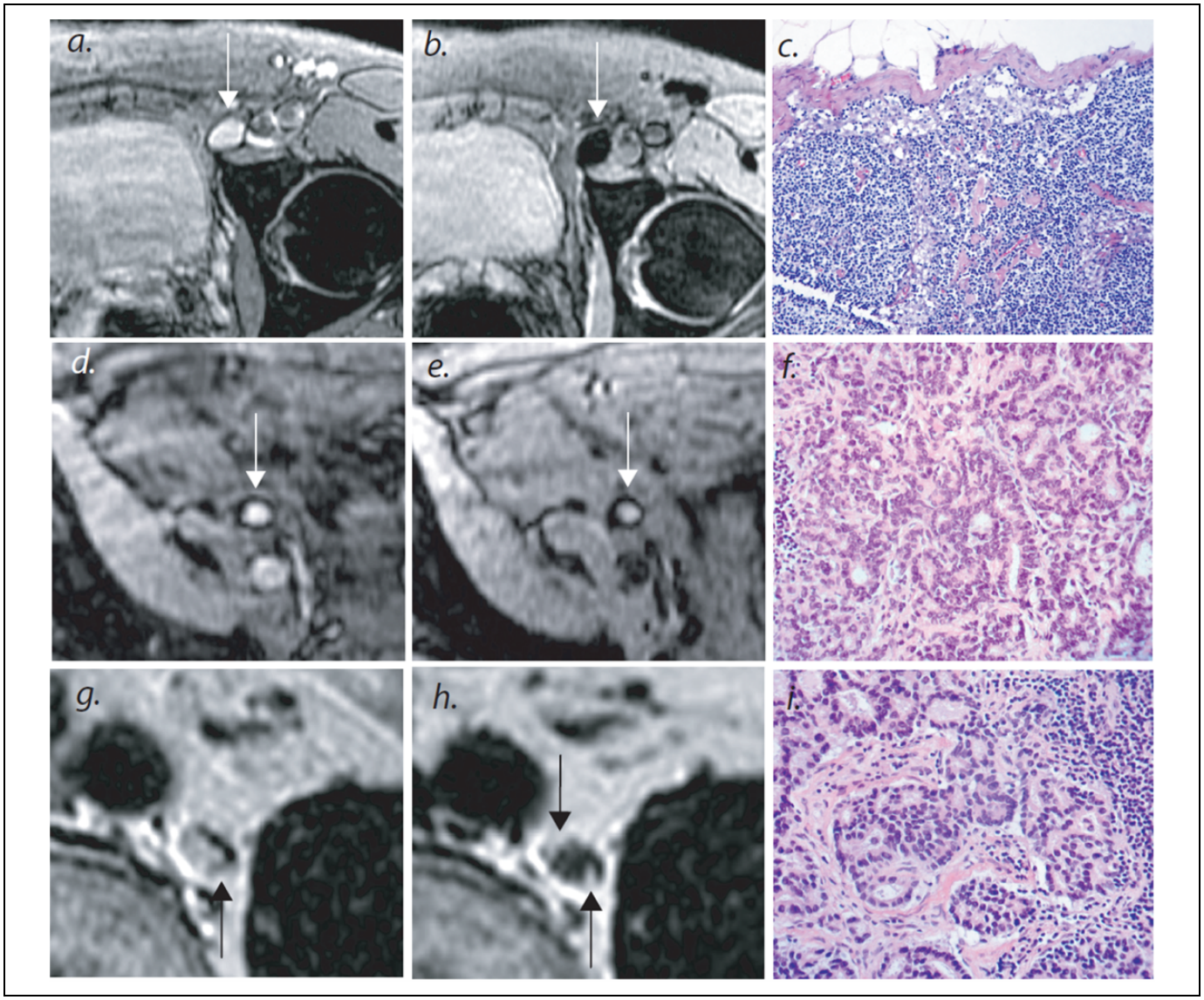

Figure 5. Magnetic resonance imaging (MRI) nodal abnormalities in 3 patients with prostate cancer. As compared with conventional MRI (panel A), MRI obtained 24 hours after the administration of lymphotropic superparamagnetic nanoparticles (panel B) shows a homogeneous decrease in signal intensity due to the accumulation of lymphotropic superparamagnetic nanoparticles in a normal lymph node in the left iliac region (arrow). Panel C shows the corresponding histologic findings (hematoxylin and eosin, ×125). Conventional MRI shows a high signal intensity in an unenlarged iliac lymph node completely replaced by tumor (arrow in panel D). Nodal signal intensity remains high (arrow in panel E). Panel F shows the corresponding histologic findings (hematoxylin and eosin, ×200). Conventional MRI shows high signal intensity in a retroperitoneal node with micrometastases (arrow in panel G). Magnetic resonance imaging with lymphotropic superparamagnetic nanoparticles demonstrates 2 hyperintense foci (arrows in panel H) within the node, corresponding to 2-mm metastases. Corresponding histologic analysis confirms the presence of adenocarcinoma within the node (panel I, hematoxylin and eosin, ×200). Reprinted with permission from Harisinghani *et al.*[97]

Conclusions

Magnetic resonance imaging is an ideal candidate for radiation treatment planning in lung cancer, although some technical limitations remain. The MRI sequences have been developed for the differentiation between malignant and benign tissues, tumor invasion, detection of metastatic lymph nodes, and delineation of OARs. These sequences can easily compete with the abilities of (PET)-CT. The main technical challenges will be real-time 4D-MRI imaging of tumor, lymph nodes, and OARs, increasing geographic accuracy of DWI images, and introducing USPIO for mediastinal staging in lung cancer. Within the next few years, these technical challenges are expected to be conquered.

Declaration of Conflicting Interests

The author(s) declared no potential conflicts of interest with respect to the research, authorship, and/or publication of this article.

Funding

The author(s) received no financial support for the research, authorship, and/or publication of this article.

References

1. Damhuis RAM, Belderbos JSA, Groen HJM. Lung cancer care in The Netherlands (Kankerzorg in Beeld: Longkanker). 2014: 50-52. Web site. https://shop.iknl.nl/shop/producten-en-diensten/nederlandse-kankerregistratie. Accessed October 23, 2015.
2. Stahel R, Peters S, Baas P, et al. Strategies for improving outcomes in NSCLC: a look to the future. *Lung Cancer*. 2013;82(3): 375-382.
3. De Ruysscher D, Belderbos J, Reymen B, et al. State of the art radiation therapy for lung cancer 2012: a glimpse of the future. *Clinical Lung Cancer*. 2013;14(2):89-95.
4. Kong FM, Ten Haken RK, Schipper MJ, et al. High-dose radiation improved local tumor control and overall survival in patients with inoperable/unresectable non-small-cell lung cancer: long-term results of a radiation dose escalation study. *Int J Radiat Oncol Biol Phys*. 2005;63(2):324-333.
5. Belderbos JS, Heemsbergen WD, De Jaeger K, Baas P, Lebesque JV. Final results of a phase I/II dose escalation trial in non-small-cell lung cancer using three-dimensional conformal radiotherapy. *Int J Radiat Oncol Biol Phys*. 2006;66(1):126-134.
6. Yuan S, Sun X, Li M, et al. A randomized study of involved-field irradiation versus elective nodal irradiation in combination with concurrent chemotherapy for inoperable stage III nonsmall cell lung cancer. *Am J Clin Oncol*. 2007;30(3):239-244.
7. Adkison JB, Khuntia D, Bentzen SM, et al. Dose escalated, hypofractionated radiotherapy using helical tomotherapy for inoperable non-small cell lung cancer: preliminary results of a risk-stratified phase I dose escalation study. *Technol Cancer Res Treat*. 2008;7(6):441-447.
8. van Baardwijk A, Reymen B, Wanders S, et al. Mature results of a phase II trial on individualised accelerated radiotherapy based on normal tissue constraints in concurrent chemo-radiation for stage III non-small cell lung cancer. *Eur J Cancer*. 2012;48(15): 2339-2346.
9. van Baardwijk A, Wanders S, Boersma L, et al. Mature results of an individualized radiation dose prescription study based on normal tissue constraints in stages I to III non-small-cell lung cancer. *J Clin Oncol*. 2010;28(8):1380-1386.
10. De Ruysscher D, van Baardwijk A, Steevens J, et al. Individualised isotoxic accelerated radiotherapy and chemotherapy are associated with improved long-term survival of patients with stage III NSCLC: a prospective population-based study. *Radiother Oncol*. 2012;102(2):228-233.
11. Mauguen A, Le Pechoux C, Saunders MI, et al. Hyperfractionated or accelerated radiotherapy in lung cancer: an individual patient data meta-analysis. *J Clin Oncol*. 2012;30(22):2788-2797.
12. Machtay M, Bae K, Movsas B, et al. Higher biologically effective dose of radiotherapy is associated with improved outcomes for locally advanced non–small cell lung carcinoma treated with chemoradiation: an analysis of the Radiation Therapy Oncology Group. *Int J Radiat Oncol Biol Phys*. 2012;82(1):425-434.
13. Bradley JD, Paulus R, Komaki R, et al. Standard-dose versus high-dose conformal radiotherapy with concurrent and consolidation carboplatin plus paclitaxel with or without cetuximab for patients with stage IIIA or IIIB non-small-cell lung cancer (RTOG 0617): a randomised, two-by-two factorial phase 3 study. *Lancet Oncol*. 2015;16(2):187-199.
14. Faivre-Finn C. Dose escalation in lung cancer: have we gone full circle? *Lancet Oncol*. 2015;16(2):125-127.
15. Nalbantov G, Kietselaer B, Vandecasteele K, et al. Cardiac comorbidity is an independent risk factor for radiation-induced lung toxicity in lung cancer patients. *Radiother Oncol*. 2013; 109(1):100-106.
16. Nestle U, Faivre-Finn C, DeRuysscher D, et al. Stereotactic body radiotherapy (SBRT) in central non-small cell lung cancer (NSCLC): solid evidence or "no-go"? *Radiother Oncol*. 2013; 109(1):178-179.
17. Lee MS, Finch W, Mahmud E. Cardiovascular complications of radiotherapy. *Am J Cardiol*. 2013;112(10):1688-1696.
18. Darby SC, Ewertz M, McGale P, et al. Risk of ischemic heart disease in women after radiotherapy for breast cancer. *N Engl J Med*. 2013;368(11):987-998.
19. Senthi S, Haasbeek CJ, Slotman BJ, Senan S. Outcomes of stereotactic ablative radiotherapy for central lung tumours: a systematic review. *Radiother Oncol*. 2013;106(3):276-282.
20. Ghobadi G, van der Veen S, Bartelds B, et al. Physiological interaction of heart and lung in thoracic irradiation. *Int J Radiat Oncol Biol Phys*. 2012;84(5):e639-e646.
21. Liu C, Gong G, Guo C, et al. The feasibility of evaluating radiation dose to the heart by integrating kilovoltage-cone beam computed tomography in stereotactic body radiotherapy of early non-small-cell lung cancer patients. *Radiat Oncol*. 2013;8:295-301.
22. De Ruysscher D, Faivre-Finn C, Nestle U, et al. European Organisation for Research and Treatment of Cancer recommendations for planning and delivery of high-dose, high-precision radiotherapy for lung cancer. *J Clin Oncol*. 2010;28(36):5301-5310.
23. Boda-Heggemann J, Lohr F, Wenz F, Flentje M, Guckenberger M. kV cone-beam CT-based IGRT: a clinical review. *Strahlenther Onkol*. 2011;187(5):284-291.
24. Langendijk JA, Lambin P, De Ruysscher D, Widder J, Bos M, Verheij M. Selection of patients for radiotherapy with protons aiming at reduction of side effects: the model-based approach. *Radiother Oncol*. 2013;107(3):267-273.
25. Wink KC, Roelofs E, Solberg T, et al. Particle therapy for non-small cell lung tumors: where do we stand? A systematic review of the literature. *Front Oncol*. 2014;4:292-292.
26. Sonke J, Belderbos J. Adaptive radiotherapy for lung cancer. *Semin Radiat Oncol*. 2010;20(2):94-106.
27. Suga K, Tsukuda T, Awaya H, et al. Impaired respiratory mechanics in pulmonary emphysema: evaluation with dynamic breathing MRI. *J Magn Reson Imaging*. 1999;10(4):510-520.
28. Plathow C, Klopp M, Fink C, et al. Quantitative analysis of lung and tumour mobility: comparison of two time-resolved MRI sequences. *Br J Radiol*. 2005;78(933):836-840.
29. Plathow C, Schoebinger M, Herth F, Tuengerthal S, Meinzer H, Kauczor H. Estimation of pulmonary motion in healthy subjects and patients with intrathoracic tumors using 3D-dynamic MRI: initial results. *Korean J Radiol*. 2009;10(6):559-567.
30. Johnson KM, Fain SB, Schiebler ML, Nagle S. Optimized 3D ultrashort echo time pulmonary MRI. *Magn Reson Med*. 2013; 70(5):1241-1250.

31. Bussels B, Goethals L, Feron M, et al. Respiration-induced movement of the upper abdominal organs: a pitfall for the three-dimensional conformal radiation treatment of pancreatic cancer. *Radiother Oncol*. 2003;68(1):69-74.
32. Feng M, Balter JM, Normolle D, et al. Characterization of pancreatic tumor motion using cine MRI: surrogates for tumor position should be used with caution. *Int J Radiat Oncol Biol Phys*. 2009;74(3):884-891.
33. Ohno Y, Adachi S, Motoyama A, et al. Multiphase ECG-triggered 3D contrast-enhanced MR angiography: utility for evaluation of hilar and mediastinal invasion of bronchogenic carcinoma. *J Magn Reson Imaging*. 2001;13(2):215-224.
34. Heerkens HD, van Vulpen M, van den Berg CAT, et al. MRI-based tumor motion characterization and gating schemes for radiation therapy of pancreatic cancer. *Radiother Oncol*. 2014; 111(2):252-257.
35. Hellwig D, Baum RP, Kirsch C. FDG-PET, PET/CT and conventional nuclear medicine procedures in the evaluation of lung cancer: a systematic review. *Nuklearmedizin*. 2009;48(2):59-69.
36. Chao F, Zhang H. PET/CT in the staging of the non-small-cell lung cancer. *J Biomed Biotechnol*. 2012;2012:1-8.
37. Devaraj A, Cook GJR, Hansell DM. PET/CT in non-small cell lung cancer staging—promises and problems. *Clin Radiol*. 2007; 62(2):97-108.
38. Cheebsumon P, Boellaard R, de Ruysscher D, et al. Assessment of tumour size in PET/CT lung cancer studies: PET- and CT-based methods compared to pathology. *EJNMMI Res*. 2012;2(1):56-64.
39. Doll C, Duncker-Rohr V, Rucker G, et al. Influence of experience and qualification on PET-based target volume delineation. When there is no expert—ask your colleague. *Strahlenther Onkol*. 2014; 190(6):555-562.
40. Zou Y, Zhang M, Wang Q, Shang D, Wang L, Yu G. Quantitative investigation of solitary pulmonary nodules: dynamic contrast-enhanced MRI and histopathologic analysis. *AJR Am J Roentgenol*. 2008;191(1):252-259.
41. Chen L, Zhang J, Bao J, et al. Meta-analysis of diffusion-weighted MRI in the differential diagnosis of lung lesions. *J Magn Reson Imaging*. 2013;37(6):1351-1358.
42. Zhang J, Cui L, Tang X, et al. DW MRI at 3.0-T versus FDG PET/CT for detection of malignant pulmonary tumors. *Int J Cancer*. 2014;134(3):606-611.
43. Ohba Y, Nomori H, Mori T, et al. Is diffusion-weighted magnetic resonance imaging superior to positron emission tomography with fludeoxyglucose F 18 in imaging non-small cell lung cancer? *J Thorac Cardiovasc Surg*. 2009;138(2):439-445.
44. Mori T, Nomori H, Ikeda K, et al. Diffusion-weighted magnetic resonance imaging for diagnosing malignant pulmonary nodules/masses: comparison with positron emission tomography. *J Thorac Oncol*. 2008;3(4):358-364.
45. Lee CU, Kollasch PD, White D, Schmitz JJ, Glockner JF, Sykes AM. Correlation of ADC values with histopathology of lung masses: preliminary results. *Proc Int Soc Magn Reson Med*. 2013;21:4107.
46. Chetley Ford J, Olsen KM, Turlington D, Ding K, Weiss E, Hugo GD, Quantitative diffusion-weighted MR imaging of lung neoplasm: a promising method for delineating active tumor. *Proc Int Soc Magn Reson Med*. 2013;21:1487.
47. Puderbach M, Hintze C, Ley S, Eichinger M, Kauczor HU, Biederer J. MR imaging of the chest: a practical approach at 1.5T. *Eur J Radiol*. 2007;64(3):345-355.
48. Yang RM, Li L, Wei XH, et al. Differentiation of central lung cancer from atelectasis: comparison of diffusion-weighted MRI with PET/CT. *PLoS One*. 2013;8(4):1-8.
49. Foroulis CN, Zarogoulidis P, Darwiche K, et al. Superior sulcus (Pancoast) tumors: current evidence on diagnosis and radical treatment. *J Thorac Dis*. 2013;5(suppl 4):s342-s358.
50. Kajiwara N, Akata S, Uchida O, et al. Cine MRI enables better therapeutic planning than CT in cases of possible lung cancer chest wall invasion. *Lung Cancer*. 2010;69(2):203-208.
51. Chang S, Hong SR, Kim YJ, et al. Usefulness of thin-section single-shot turbo spin echo with half-Fourier acquisition in evaluation of local invasion of lung cancer. *J Magn Reson Imaging*. 2014;41(3):747-754.
52. Hong YJ, Hur J, Lee HJ, et al. Respiratory dynamic magnetic resonance imaging for determining aortic invasion of thoracic neoplasms. *J Thorac Cardiovasc Surg*. 2014;148(2): 644-650.
53. Bruzzi JF, Komaki R, Walsh GL, et al. Imaging of non–small cell lung cancer of the superior sulcus: part 1: anatomy, clinical manifestations, and management. *Radiographics*. 2008;28(2): 551-560.
54. Ohno Y, Hatabu H, Takenaka D, et al. Metastases in mediastinal and hilar lymph nodes in patients with non-small cell lung cancer: quantitative and qualitative assessment with STIR turbo spin-echo MR imaging. *Radiology*. 2004;231(3):872-879.
55. Ohno Y, Koyama H, Yoshikawa T, et al. N stage disease in patients with non-small cell lung cancer: efficacy of quantitative and qualitative assessment with STIR turbo spin-echo imaging, diffusion-weighted MR imaging, and fluorodeoxyglucose PET/CT. *Radiology*. 2011;261(2):605-615.
56. Kim YN, Yi CA, Lee KS, et al. A proposal for combined MRI and PET/CT interpretation criteria for preoperative nodal staging in non-small-cell lung cancer. *Eur Radiol*. 2012;22(7): 1537-1546.
57. Peerlings J, Troost EGC, Nelemans PJ, et al. The diagnostic value of MRI in staging (non-)metastatic lymph nodes in patients with non-small cell lung cancer: a meta-analysis. Accepted for publication.
58. Harisinghani M, Ross RW, Guimaraes AR, Weissleder R. Utility of a new bolus-injectable nanoparticle for clinical cancer staging. *Neoplasia*. 2007;9(12):1160-1165.
59. Islam T, Harisinghani MG. Overview of nanoparticle use in cancer imaging. *Cancer Biomark*. 2009;5(2):61-67.
60. Kong FM, Ritter T, Quint DJ, et al. Consideration of dose limits for organs at risk of thoracic radiotherapy: atlas for lung, proximal bronchial tree, esophagus, spinal cord, ribs, and brachial plexus. *Int J Radiat Oncol Biol Phys*. 2011;81(5):1442-1457.
61. Cai J, Sheng K, Sheehan JP, Benedict SH, Larner JM, Read PW. Evaluation of thoracic spinal cord motion using dynamic MRI. *Radiother Oncol*. 2007;84(3):279-282.
62. Hoover DA, Capaldi DP, Sheikh K, et al. Functional lung avoidance for individualized radiotherapy (FLAIR): study protocol for a randomized, double-blind clinical trial. *BMC Cancer*. 2014;14: 934.

63. Fox MS, Ouriadov A, Thind K, et al. Detection of radiation induced lung injury in rats using dynamic hyperpolarized (129)Xe magnetic resonance spectroscopy. *Med Phys*. 2014; 41(7):072302.
64. Allen AM, Albert M, Caglar HB, et al. Can hyperpolarized helium MRI add to radiation planning and follow-up in lung cancer? *J Appl Clin Med Phys*. 2011;12(2):169-183.
65. Bruzzi JF, Komaki R, Walsh GL, et al. Imaging of non–small cell lung cancer of the superior sulcus: part 2: initial staging and assessment of resectability and therapeutic response. *Radiographics*. 2008;28(2):561-572.
66. Tryggestad E, Flammang A, Han-Oh S, et al. Respiration-based sorting of dynamic MRI to derive representative 4D-MRI for radiotherapy planning. *Med Phys*. 2013;40(5):051909-051909.
67. Cai J, Chang Z, Wang Z, Paul Segars W, Yin FF. Four-dimensional magnetic resonance imaging (4D-MRI) using image-based respiratory surrogate: a feasibility study. *Med Phys*. 2011;38(12):6384-6394.
68. Sawant A, Keall P, Pauly KB, et al. Investigating the feasibility of rapid MRI for image-guided motion management in lung cancer radiotherapy. *Biomed Res Int*. 2014;2014:485067-485067.
69. Hu Y, Caruthers SD, Low DA, Parikh PJ, Mutic S. Respiratory amplitude guided 4-dimensional magnetic resonance imaging. *Int J Radiat Oncol Biol Phys*. 2013;86(1):198-204.
70. Padovani B, Mouroux J, Seksik L, et al. Chest wall invasion by bronchogenic carcinoma: evaluation with MR imaging. *Radiology*. 1993;187(1):33-38.
71. Kajiwara N, Akata S, Uchida O, et al. Cine MRI enables better therapeutic planning than CT in cases of possible lung cancer chest wall invasion. *Lung Cancer*. 2010;69(2):203-208.
72. Mahesh M, Detorie N, Ford EC. Technical aspects of respiration-correlated 4-D CT for radiation therapy. *J Am Coll Radiol*. 2007; 4(3):192-194.
73. Wu Y, Li P, Zhang H, et al. Diagnostic value of fluorine 18 fluorodeoxyglucose positron emission tomography/computed tomography for the detection of metastases in non-small-cell lung cancer patients. *Int J Cancer*. 2013;132(2):e37-e47.
74. Lv YL, Yuan DM, Wang K, et al. Diagnostic performance of integrated positron emission tomography/computed tomography for mediastinal lymph node staging in non-small cell lung cancer: a bivariate systematic review and meta-analysis. *J Thorac Oncol*. 2011;6(8):1350-1358.
75. Zhao L, He ZY, Zhong XN, Cui ML. (18)FDG-PET-CT for detection of mediastinal nodal metastasis in non-small cell lung cancer: a meta-analysis. *Surg Oncol*. 2012;21(3):230-236.
76. Wu LM, Xu JR, Gu HY, et al. Preoperative mediastinal and hilar nodal staging with diffusion-weighted magnetic resonance imaging and fluorodeoxyglucose positron emission tomography/computed tomography in patients with non-small-cell lung cancer: which is better? *J Surg Res*. 2012;178(1):304-314.
77. van Elmpt W, Ollers M, van Herwijnen H, et al. Volume or position changes of primary lung tumor during (chemo-)radiotherapy cannot be used as a surrogate for mediastinal lymph node changes: the case for optimal mediastinal lymph node imaging during radiotherapy. *Int J Radiat Oncol Biol Phys*. 2011;79(1): 89-95.
78. Schaake EE, Belderbos JS, Buikhuisen WA, Rossi MM, Burgers JA, Sonke JJ. Mediastinal lymph node position variability in non-small cell lung cancer patients treated with radical irradiation. *Radiother Oncol*. 2012;105(2):150-154.
79. van Rossum PS, van Lier AL, Lips IM, et al. Imaging of oesophageal cancer with FDG-PET-CT and MRI. *Clin Radiol*. 2015; 70(1):81-95.
80. Giraud P, De Rycke Y, Dubray B, et al. Conformal radiotherapy (CRT) planning for lung cancer: analysis of intrathoracic organ motion during extreme phases of breathing. *Int J Radiat Oncol Biol Phys*. 2001;51(4):1081-1092.
81. Dieleman EM, Senan S, Vincent A, Lagerwaard FJ, Slotman BJ, van Sornsen de Koste JR. Four-dimensional computed tomographic analysis of esophageal mobility during normal respiration. *Int J Radiat Oncol Biol Phys*. 2007;67(3):775-780.
82. Pracht ED, Arnold JF, Wang T, Jakob PM. Oxygen-enhanced proton imaging of the human lung using T2. *Magn Reson Med*. 2005;53(5):1193-1196.
83. Biederer J. General requirements of MRI of the lung and suggested standard protocol. In: Kauczor HU, ed. *MRI of the Lung*. Berlin Heidelberg: Springer-Verlag; 2009:3-16.
84. Raaijmakers AJ, Raaymakers BW, Lagendijk JJ. Integrating a MRI scanner with a 6 MV radiotherapy accelerator: dose increase at tissue-air interfaces in a lateral magnetic field due to returning electrons. *Phys Med Biol*. 2005;50(7):1363-1376.
85. Constantin DE, Fahrig R, Keall PJ. A study of the effect of in-line and perpendicular magnetic fields on beam characteristics of electron guns in medical linear accelerators. *Med Phys*. 2011;38(7): 4174-4185.
86. Lagendijk JJ, Raaymakers BW, Raaijmakers AJ, et al. MRI/linac integration. *Radiother Oncol*. 2008;86(1):25-29.
87. Fallone BG, Murray B, Rathee S, et al. First MR images obtained during megavoltage photon irradiation from a prototype integrated linac-MR system. *Med Phys*. 2009;36(6):2084-2088.
88. Stemkens B, Tijssen RH, de Senneville BD, Lagendijk JJW, van den Berg CAT. Estimating dynamic 3D abdominal motion for radiation dose accumulation mapping using a PCA-based model and 2D navigators. In: Proceedings from the 23th International Society of Magnetic Resonance in Medicine; 2015; Toronto, Canada:1867.
89. Yamamoto T, Langner BW, Loo U Jr., Shen J, Keall PJ. Retrospective analysis of artifacts in four-dimensional CT images of 50 abdominal and thoracic radiotherapy patients. *Int J Radiat Oncol Biol Phys*. 2008;72(4):1250-1258.
90. McClelland J. Estimating internal respiratory motion from respiratory surrogate signals using correspondence models. In: Ehrhardt J, Lorenz C, eds. *4D Modeling and Estimation of Respiratory Motion for Radiation Therapy*. Berlin Heidelberg: Springer-Verlag; 2013:187-213.
91. Mishra P, Li R, Mak RH, et al. An initial study on the estimation of time-varying volumetric treatment images and 3D tumor localization from single MV cine EPID images. *Med Phys*. 2014; 41(8):081713-081713.
92. King AP, Buerger C, Tsoumpas C, Marsden PK, Schaeffter T. Thoracic respiratory motion estimation from MRI using a statistical model and a 2-D image navigator. *Med Image Anal*. 2012; 16(1):252-264.

93. Chun SY, Reese TG, Ouyang J, et al. MRI-based nonrigid motion correction in simultaneous PET/MRI. *J Nucl Med*. 2012;53(8):1284-1291.
94. Giannarini G, Zazzara M, Rossanese M, et al. Will multi-parametric magnetic resonance imaging be the future tool to detect clinically significant prostate cancer? *Front Oncol*. 2014;4:294-294.
95. Coffey N, Schieda N, Cron G, Gulavita P, Mai KT, Flood TA. Multi-parametric (mp) MRI of prostatic ductal adenocarcinoma. *J Magn Reson Imaging*. 2015;41(6):1639-1645
96. Dikaios N, Alkalbani J, Sidhu HS, et al. Logistic regression model for diagnosis of transition zone prostate cancer on multi-parametric MRI. *Eur Radiol*. 2014;25(2):523-532.
97. Harisinghani MG, Barentsz J, Hahn PF, et al. Noninvasive detection of clinically occult lymph-node metastases in prostate cancer. *N Engl J Med*. 2003;348(25):2491-2499.
98. Fortuin AS, Smeenk RJ, Meijer HJ, Witjes AJ, Barentsz JO. Lymphotropic nanoparticle-enhanced MRI in prostate cancer: value and therapeutic potential. *Curr Urol Rep*. 2014;15(3):389-389.
99. Fortuin AS, Deserno WM, Meijer HJ, et al. Value of PET/CT and MR lymphography in treatment of prostate cancer patients with lymph node metastases. *Int J Radiat Oncol Biol Phys*. 2012; 84(3):712-718.
100. Nguyen BC, Stanford W, Thompson BH, et al. Multicenter clinical trial of ultrasmall superparamagnetic iron oxide in the evaluation of mediastinal lymph nodes in patients with primary lung carcinoma. *J Magn Reson Imaging*. 1999;10(3):468-473.
101. Eisenhauer EA, Therasse P, Bogaerts J, et al. New response evaluation criteria in solid tumours: revised RECIST guideline (version 1.1). *Eur J Cancer*. 2009;45(2):228-247.
102. Ratain MJ, Eckhardt SG. Phase II studies of modern drugs directed against new targets: if you are fazed, too, then resist RECIST. *J Clin Oncol*. 2004;22(22):4442-4445.
103. Wahl RL, Jacene H, Kasamon Y, Lodge MA. From RECIST to PERCIST: evolving considerations for PET response criteria in solid tumors. *J Nucl Med*. 2009;50(suppl 1):122s-150s.
104. Vos CG, Dahele M, van Sornsen de Koste JR, et al. Semiautomated volumetric response evaluation as an imaging biomarker in superior sulcus tumors. *Strahlenther Onkol*. 2014;190(2): 204-209.
105. Chen HH, Chiu NT, Su WC, Guo HR, Lee BF. Prognostic value of whole-body total lesion glycolysis at pretreatment FDG PET/CT in non-small cell lung cancer. *Radiology*. 2012;264(2): 559-566.
106. Zhang H, Wroblewski K, Liao S, et al. Prognostic value of metabolic tumor burden from (18)F-FDG PET in surgical patients with non-small-cell lung cancer. *Acad Radiol*. 2013; 20(1):32-40.
107. Ohno Y, Koyama H, Yoshikawa T, et al. Diffusion-weighted MRI versus 18F-FDG PET/CT: performance as predictors of tumor treatment response and patient survival in patients with non-small cell lung cancer receiving chemoradiotherapy. *AJR Am J Roentgenol*. 2012;198(1):75-82.
108. de Langen AJ, van den Boogaart V, Lubberink M, et al. Monitoring response to antiangiogenic therapy in non–small cell lung cancer using imaging markers derived from PET and dynamic contrast-enhanced MRI. *J Nucl Med*. 2011;52(1):48-55.
109. Shanbhogue AK, Karnad AB, Prasad SR. Tumor response evaluation in oncology: current update. *J Comput Assist Tomogr*. 2010;34(4):479-484.
110. Cho SH, Kim GC, Jang YJ, et al. Locally advanced rectal cancer: post-chemoradiotherapy ADC histogram analysis for predicting a complete response. *Acta Radiol*. 2015;56(9):1042-1050.
111. Beets-Tan RG, Beets GL. MRI for assessing and predicting response to neoadjuvant treatment in rectal cancer. *Nat Rev Gastroenterol Hepatol*. 2014;11(8):480-488.
112. Lambregts DM, Vandecaveye V, Barbaro B, et al. Diffusion-weighted MRI for selection of complete responders after chemoradiation for locally advanced rectal cancer: a multicenter study. *Ann Surg Oncol*. 2011;18(8):2224-2231.
113. Intven M, Reerink O, Philippens ME. Dynamic contrast enhanced MR imaging for rectal cancer response assessment after neo-adjuvant chemoradiation. *J Magn Reson Imaging*. 2015;41(6):1646-1653.
114. Tsuchida T, Morikawa M, Demura Y, Umeda Y, Okazawa H, Kimura H. Imaging the early response to chemotherapy in advanced lung cancer with diffusion-weighted magnetic resonance imaging compared to fluorine-18 fluorodeoxyglucose positron emission tomography and computed tomography. *J Magn Reson Imaging*. 2013;38(1):80-88.
115. Yabuuchi H, Hatakenaka M, Takayama K, et al. Non-small cell lung cancer: detection of early response to chemotherapy by using contrast-enhanced dynamic and diffusion-weighted MR imaging. *Radiology*. 2011;261(2):598-604.